Intermittency, Log-Normal Statistics, and Multifractal Cascade Process in High-Resolution Satellite Images of Cloud Structure

A. Arneodo,[1] N. Decoster,[1] and S. G. Roux[2]
[1]*Centre de Recherche Paul Pascal, Avenue Schweitzer, 33600 Pessac, France*
[2]*Climate & Radiation Branch, NASA Goddard Space Flight Center, Greenbelt, Maryland 20771*
(Received 11 January 1999)

We apply a wavelet based deconvolution method to LANDSAT satellite images of cloudy scenes. This method proves to be very efficient to disentangle the convective cell anisotropic texture from the isotropic scale invariant background radiance fluctuations. We show that the experimental data do not allow us to discriminate between various phenomenological cascade models that account for intermittency and their log-normal approximations. We comment on the multifractal properties of stratocumulus radius fields comparatively to fully developed turbulence data.

PACS numbers: 92.60.Nv, 47.27.Jv, 47.53.+n, 92.60.Jq

The problem of nonlinear variability over a wide range of scales has been considered for a long time with respect to the highly intermittent nature of turbulent flows [1]. Special attention has been paid to their asymptotic and possibly universal behavior when the dissipation length goes to zero. The atmosphere is a huge natural laboratory where high Reynolds number turbulent dynamics can be studied. Clouds are the most obvious manifestations of the Earth's turbulent atmospheric dynamics [2]. By modulating the input of the solar radiation, they play a critical role in the maintenance of the Earth's climate. They are also one of the main sources of uncertainty in current climate modeling [3]. Until quite recently, the internal structure of clouds was probed by balloons or aircrafts that penetrate the cloud layer, revealing an extreme variability of 1D cuts of some cloud fields, e.g., liquid water content (LWC) [4]. An alternative to *in situ* probing is to use high-resolution satellite imagery that now provides direct information about the fluctuations in LWC in the depth of clouds. These sophisticated remote sensing systems have confirmed the intermittent character of these fluctuations [5] which is hardly a surprise in such highly turbulent environments.

Since Parisi and Frisch [6], it has now become routine to apply multifractal concepts to characterizing the intermittent behavior of velocity or other observable turbulent fields. As emphasized in Ref. [7], a very efficient alternative to the commonly used structure function method [1] consists in using the continuous wavelet transform (WT). Actually, the WT skeleton defined by the wavelet transform modulus maxima (WTMM) provides an adaptive space-scale partitioning from which one can extract the entire $D(h)$ singularity spectrum via the scaling exponents $\tau(p)$ of some partition functions defined on the WT skeleton. Very recently, the WTMM method has been generalized to multifractal image analysis [8]. Preliminary application to LANDSAT scene of a marine stratocumulus (Sc) yields a $\tau(p)$ spectrum that clearly displays a nonlinear behavior, the hallmark of multifractality [8]. A comparative statistical analysis of stochastic models of clouds [9,10] legitimates the relevance of the multifractal description of intermittency in cloud satellite images. But multifractal spectra are nothing else than thermodynamical potentials which contain only some degenerate information about the underlying multiplicative process. Thus, if one can compare the experimental $\tau(p)$ and $D(h)$ spectra to the predictions of various cloud models, by no means will they provide a selective test to discriminate between these models.

In the context of fully developed turbulence, Castaing *et al.* [11] have proposed some original approach of intermittency. It amounts to modeling the evolution of the velocity increment probability density function (pdf) from Gaussian at large scales to more intermittent profiles with stretched exponential-like tails at smaller scales, by a functional equation that relates two scales $l' > l$ using a kernel G:

$$P_l(\delta v) = \int G_{ll'}(\ln\sigma)\,\frac{1}{\sigma}\,P_{l'}\left(\frac{\delta v}{\sigma}\right) d\ln\sigma\,. \qquad (1)$$

Indeed most of the well-known multiplicative cascade models, including the log-stable [9,12] and the log-infinitely divisible [13] cascade models, can be reformulated within this approach. This amounts (i) to specify the shape of the kernel $G(u)$ which is determined by the nature of the elementary step in the cascade and (ii) to define the way $G_{ll'}$ depends upon l and l'. From Eq. (1), one can show that, for any decreasing sequence of scales $(l_1, l_2, \ldots, l_n)$, one has $G_{l_n l_1} = G_{l_n l_{n-1}} \otimes \cdots \otimes G_{l_2 l_1}$, where $\otimes$ denotes the convolution product. The cascade is *continuously self-similar* [11,13(b)] if there exists a positive, monotonous function $S(l)$, such that $G_{ll'}(u) = G[u, S(l, l')]$, where $S(l, l') = S(l) - S(l')$. The cascade is *scale-similar* [13(a)] if the number of cascade steps from l' to l behaves as $S(l, l') = \ln(l'/l)$. In Ref. [11], Castaing *et al.* mainly focused on the scaling behavior of the variance of G. In Ref. [14], a generalization of Eq. (1) to the WT of the velocity field has been shown to provide access to the entire shape of G. The aim of

the present study is to extend this wavelet-based deconvolution technique from 1D to 2D signals with the specific goal to improve statistical characterization of high-resolution satellite images, a prerequisite for developing better models of cloud structure and furthering our understanding of cloud-radiation interaction.

In recent years, there has been increasing interest in the application of the WT to image processing. In Ref. [15], Mallat *et al.* have extended the WTMM representation in 2D in the spirit of Canny's multiscale edge detectors. The idea is to first smooth the digital image by convolution with a filter, then compute the gradient of the smooth signal. Define two wavelets: $\psi_1(x,y) = \partial\theta(x,y)/\partial x$ and $\psi_2(x,y) = \partial\theta(x,y)/\partial y$, where $\theta(x,y)$ is a 2D smoothing function well localized around $x = y = 0$. For any function $f(x,y) \in L^2(\mathbb{R}^2)$, the WT defined with respect to ψ_1 and ψ_2 can be expressed as a vector [15]:

$$\mathbf{T}_\psi[f](\mathbf{b},a) = \nabla\{T_\theta[f](\mathbf{b},a)\}, \qquad (2)$$

where $T_\theta[f](\mathbf{b},a) = a^{-2}\iint_{-\infty}^{+\infty}\theta(\frac{\mathbf{r}-\mathbf{b}}{a})f(\mathbf{r})\,d^2\mathbf{r}$. If θ is just a Gaussian $\theta(\mathbf{r}) = \exp(-\mathbf{r}^2/2)$, then Eq. (2) defines the 2D WT as the gradient vector of $f(\mathbf{r})$ smoothed by dilated versions $\theta(\mathbf{r}/a)$ of this filter [15]. At a given scale a, the WTMM are defined by the positions $\mathbf{b}$ where the WT modulus $\mathcal{M}_\psi[f](\mathbf{b},a)$ is locally maximum in the direction $\mathcal{A}_\psi[f](\mathbf{b},a)$ of the gradient vector $\mathbf{T}_\psi[f]$. As reported in Ref. [8], when analyzing rough surfaces, these WTMM lie on connected chains. Then the WTMM maxima (WTMMM) are identified as the local maxima of $\mathcal{M}$ along the WTMM chains (Fig. 1). The generalized 2D WTMM method consists in computing partition functions from these WTMMM [8(b)]. These WTMMM are disposed along connected curves across scales. The WT skeleton defined by these maxima lines contains *a priori* all the information about the hierarchical organization of the singularities of the function $f(x,y)$. In particular, one can prove [8(b)] that, provided the first n_ψ moments of ψ are zero, then $\mathcal{M}_\psi \sim a^{h(\mathbf{r}_0)}$ along a maxima line pointing to the point $\mathbf{r}_0$ in the limit $a \to 0$, where $h(\mathbf{r}_0)$ ($< n_\psi$) is the local Hölder exponent of f.

Stratocumulus are one of the most studied cloud types [4,5]. Being at once persistent and horizontal extended, marine Sc layers are responsible for a large portion of the Earth's global albedo, hence, its overall energy balance. We start with a large ($\simeq 196 \times 168$ km^2) cloudy LANDSAT scene captured with the Thematic Mapper camera ($\simeq$28 m resolution) in the 0.5–0.6 μm channel during the First ISCCP Regional experiment off the coast of San Diego, California, on 7 July 1987. Figure 1(a) shows a typical 1024×1024 pixels portion of the original image where quasinadir viewing radiance at satellite level is digitized on an eight-bit grey scale. To master edge effects, we select 25 overlapping 1024×1024 pixels subscenes in the cloudy region. In Fig. 1(b) we show the WT modulus of a 256×256 pixels portion, computed at scale $a = 68$ (1904 m) with a first-order analyzing wavelet ($n_\psi = 1$) taking θ as a Gaussian. The corresponding WTMM chains are shown in Fig. 1(c). The local maxima of $\mathcal{M}_\psi$ along these chains are indicated by ($\times$). As shown in Fig. 1(d), when decreasing a, the number of WTMMM increases like a^{-2}, which means that the support of the singularities of the radiance field has a dimension $d = 2$. In Figs. 2(a) and 2(b) are reported the results of the computation of the WTMMM pdf's $P_a(\mathcal{M})$ and $P_a(\mathcal{A})$ for three different scales. In Fig. 2(c), the pdf's of $\mathcal{M}$ are revisited when using a logarithmic representation. The first important message which comes out from our analysis is illustrated in Fig. 2(d): $P_a(\mathcal{M},\mathcal{A}) = P_a(\mathcal{M})P_a(\mathcal{A})$; i.e., the modulus and the argument of the WTMMM are independent whatever the scale a, from $a_{\min} \simeq 13$ (364 m), below which our analyzing wavelet is not resolved [16], up to $a_{\max} \simeq 208$ (5824 m), the largest scale for which $P_a(\mathcal{M})$ and $P_a(\mathcal{A})$ are still well defined distributions.

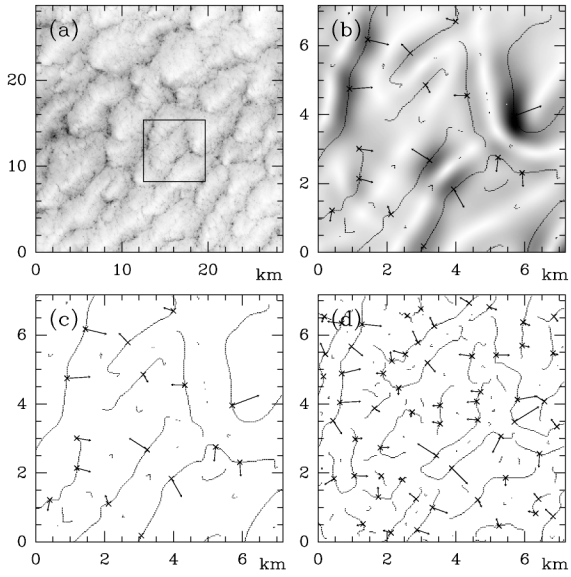

FIG. 1. 2D WT analysis of a marine Sc LANDSAT image. $\theta(x,y)$ is Gaussian. (a) 256 grey-scale coding of a 1024×1024 pixels portion of the original radiance image. (b) WT modulus of the 256×256 pixels portion delimited by the square in (a), $a = 68$ (1904 m); $\mathcal{M}_\psi$ is coded using 32 grey levels from white ($\mathcal{M}_\psi = 0$) to black ($\max\mathcal{M}_\psi$). (c) The corresponding WTMM chains; the local maxima of $\mathcal{M}_\psi$ along these chains are indicated by ($\times$) from which originates the vector $\mathbf{T}_\varphi[f]$. (d) Same as (c) but at scale $a = 34$ (952 m).

As shown in Fig. 2(b), $P_a(\mathcal{A})$ is clearly scale dependent with some evidence of anisotropy enhancement when going from small to large scales. Two peaks around the values $\mathcal{A} \simeq -\pi/10$ and $9\pi/10$ become more and more pronounced as the signature of a privileged direction in the analyzed images. As seen Fig. 1(a), this direction is nothing but the perpendicular to the mean direction of the convective rolls that are generally aligned to the wind direction. Thus, at large scales, the WT microscope is sensitive to the convective cell texture, a rather regular pattern superimposed to the background

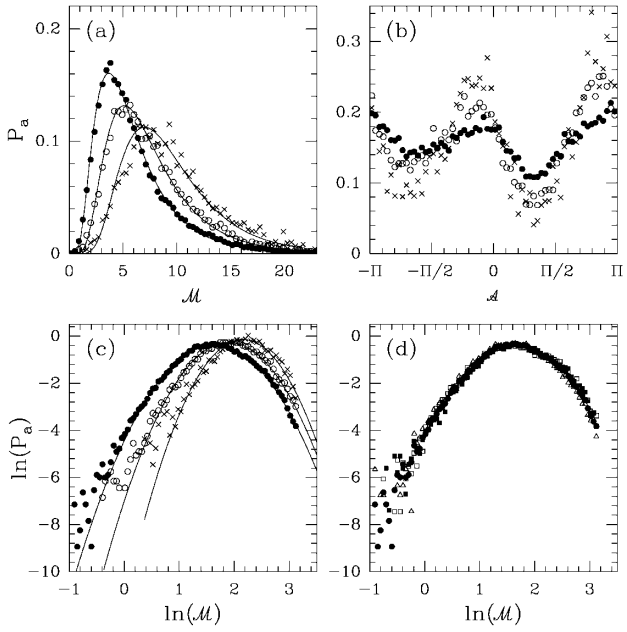

FIG. 2. pdf's of WTMMM coefficients at scales $a = 17$ (●), 34 (○), and 68 (×). $\theta(x, y)$ is Gaussian. (a) $P_a(\mathcal{M})$ vs $\mathcal{M}$. (b) $P_a(\mathcal{A})$ vs $\mathcal{A}$. (c) $\ln[P_a(\ln\mathcal{M})]$ vs $\ln\mathcal{M}$. (d) $\ln[P_a(\ln\mathcal{M})]$ vs $\ln\mathcal{M}$ at scale $a = 17$, when conditioning the modulus $\mathcal{M}$ to the argument $\mathcal{A} = 0 \pm \pi/8$ (□), $\pi/4 \pm \pi/8$ (■), and $\pi/2 \pm \pi/8$ (Δ). The solid lines in (a) and (c) correspond to the log-normal approximation of the histograms.

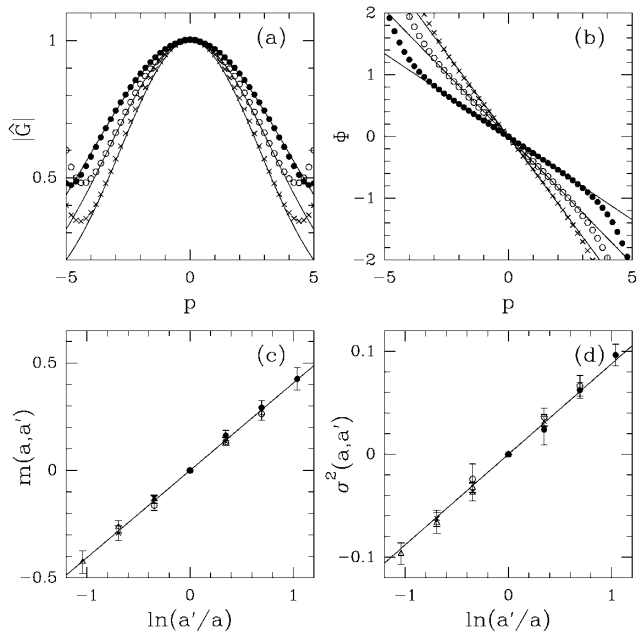

FIG. 3. (a) $|\hat{G}_{aa'}|$ vs p; (b) $\phi_{aa'} = \arctan(\mathrm{Im}\hat{G}_{aa'}/\mathrm{Re}\hat{G}_{aa'})$ vs p, for $a = 28$, $a' = 56$ (●), $a = 19$, $a' = 56$ (○), and $a = 19$, $a' = 76$ (×). The solid lines represent fits of the data with a log-normal kernel. (c) $m(a, a') = -\partial\,\mathrm{Im}(\hat{G}_{aa'})/\partial p|_{p=0}$ vs $\ln(a'/a)$; (d) $\sigma^2(a, a') = \partial^2(\ln|\hat{G}_{aa'}|)/\partial p^2|_{p=0}$ vs $\ln(a'/a)$, for $a' = 28$ (●), 39 (○), 56 (×), and 79 (Δ). The solid lines correspond to linear regression fits with slopes $m = 0.40 \pm 0.02$ and $\sigma^2 = 0.084 \pm 0.06$, respectively.

radiance fluctuations. Note that the number of corresponding WTMMM with an argument $\mathcal{A} \simeq -\pi/10$ or $9\pi/10$ increases similar to a^{-1} (the dimension of the edges of the rolls is $d = 1$), i.e., much slower than a^{-2} as observed for the other WTMMM. What Fig. 2(d) tells us is that this progressive extinction of the convective cell texture anisotropy does not affect the scaling properties of $P_a(\mathcal{M})$. When plotting $\ln P_a(\ln\mathcal{M})$ vs $\ln\mathcal{M}$, one gets in Fig. 2(c) the remarkable result that, for any scale $a \in [a_{\min}, a_{\max}]$, all the data points fall, within a good approximation, on a parabola, which suggests that the WTMMM have a log-normal statistics.

Along the line of the Castaing *et al.* ansatz [Eq. (1)], $P_a(\mathcal{M})$ at scale a can be expressed as a weighted sum of dilated pdf's at a different scale $a' > a$. Let $M(p, a) = \int e^{ip\ln\mathcal{M}} P_a(\mathcal{M})\, d\mathcal{M}$ be the characteristic function associated with the logarithm of the WTMMM at scale a; then the Fourier transform $\hat{G}$ of the kernel G can be computed on $\hat{G}_{aa'}(p) = M(p, a)/M(p, a')$, provided $M(p, a')$ do not vanish [14]. From the convolution property of G and the additivity of the function S, the cascade is continuously self-similar if $\hat{G}_{aa'}$ can be expressed as

$$\hat{G}_{aa'}(p) = \hat{G}(p)^{S(a,a')}. \tag{3}$$

Our numerical results for the modulus and the phase of $\hat{G}_{aa'}(p)$ are reported in Fig. 3. As long as $a_{\min} \lesssim a < a' \lesssim a_{\max}$, this kernel is very well fitted, for $-4 \leq p \leq 4$, by the Fourier transform of a log-normal kernel [14]: $\hat{G}_{aa'}(p) = \exp[(-imp - \frac{\sigma^2 p^2}{2})S(a, a')]$. Thus, with the available statistics, one cannot distinguish the various log-infinitely divisible [13] and log-stable [9] cascade models from their log-normal approximations. This result is quite consistent with the observation that $P_a(\mathcal{M})$ has nearly a log-normal shape [Fig. 2(c)]. In order to test scale similarity, we plot, in Figs. 3(c) and 3(d), $m(a, a') = -\partial\,\mathrm{Im}(\hat{G}_{aa'})/\partial p|_{p=0}$ and $\sigma^2(a, a') = \partial^2(\ln|\hat{G}_{aa'}|)/\partial p^2|_{p=0}$ as functions of $\ln(a'/a)$. It is striking that the data obtained, when fixing the largest scale a' and varying the smallest one a, all fall on the same unique straight line whatever a'. This is an unambiguous experimental evidence for scale invariance: The number of cascade steps scales as expected $S(a, a') = \ln(a'/a)$. From the slope of $m(a, a')$ and $\sigma^2(a, a')$, one gets $m = 0.40 \pm 0.02$ and $\sigma^2 = 0.084 \pm 0.006$, respectively. In Fig. 4(a) are shown the $\tau(p)$ spectra computed with the 2D WTMM method with a first-order ($n_\psi = 1$), and a third-order ($n_\psi = 3$) analyzing wavelet. The data clearly do not depend upon the shape of ψ as it should be for a scale-invariant self-similar process [7]. Moreover, the experimental spectra remarkably coincide with the quadratic log-normal prediction $\tau(p) = mp - \sigma^2 p^2/2 - 2$, when using the parameter values extracted from the kernel in Fig. 3. The corresponding $D(h)$ singularity spectrum is shown in Fig. 4(b). Up to the numerical uncertainty,

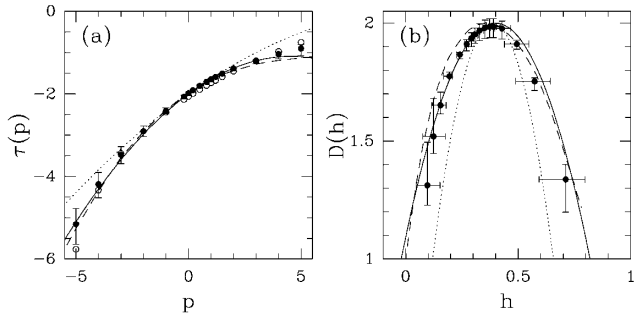

FIG. 4. Multifractal spectra computed with a first-order (●) (θ = Gaussian) and a third-order (○) (θ = second derivative of Gaussian) analyzing wavelet. (a) $\tau(p)$ vs p. (b) $D(h)$ vs h. The solid lines correspond to the log-normal predictions. The multifractal spectra of velocity (dotted line) and temperature (dashed line) fluctuations in fully developed 3D turbulence are shown for comparison.

its overall parabolic shape has its maximum equal to 2 for $h = m = 0.40$. This is a strong indication that the radiance field of marine Sc is singular everywhere and displays isotropic multifractal properties. Let us point out that, from the estimate of $\tau(2) = -1.37$, one deduces the following value $\beta = 4 + \tau(2) = 2.63$ for the scaling exponent of the spectral density, in good agreement with previous estimates [4,5].

In summary, we have shown that the anisotropic texture induced by the convective rolls is nothing but a superimposed structure that does not affect the isotropic scale-invariant properties displayed by the radiance fluctuations. These fluctuations are found to have log-normal statistics on the widest range of scales accessible to our 2D WT microscope. Moreover, our findings for the kernel $G_{aa'}$ strongly indicate that intermittency in the marine Sc radiance field can be understood in terms of a continuous self-similar log-normal multiplicative process. Let us point out that a previous 1D WT analysis of the velocity fluctuations in high Reynolds number turbulence has come to similar conclusions [14]. In Fig. 4 are shown for comparison the $\tau(p)$ and $D(h)$ spectra obtained for a turbulent velocity signal recorded at the Modane wind tunnel ($R_\lambda \simeq 2000$) [14]. [Indeed $\tau(p) - 1$ and $D(h) + 1$ are represented in order to compare 1D to 2D data.] These quadratic spectra differ from the results obtained for the Sc cloud. They have a common feature; i.e., the most frequent Hölder exponent in the radiance field $h = m = \partial\tau/\partial p|_{p=0} = 0.40 \pm 0.02$ is undistinguishable from the corresponding exponent $m = 0.39 \pm 0.01$ found for the turbulent velocity field. The main difference comes from the nonlinear term in $\tau(p)$ which is much stronger ($\sigma^2 = 0.084 \pm 0.006$) for the cloud than for the turbulent velocity ($\sigma^2 = 0.036 \pm 0.004$). This is the signature that the radiance field is more intermittent than the velocity field. As seen in Fig. 4(b), the $D(h)$ spectrum is unambiguously wider for the former than for the later. In Fig. 4 are also reported the multifractal spectra of the temperature fluctuations recorded in a $R_\lambda = 400$ turbulent flow [17]. These spectra are remarkably similar to those of the marine Sc radiance field. This suggests that radiance intermittency captured by the LANDSAT satellite is statistically equivalent to the intermittency of a passive scale in fully developed 3D turbulence.

We thank E. Bacry, R. Cahalan, A. Davis, A. Marshak, and J. F. Muzy for stimulating discussions. We are very grateful to Y. Gagne, Y. Malecot, and S. Ciliberto for the permission to use their turbulence data. This work was supported by NATO (Grant No. CRG 960176).

[1] U. Frisch, *Turbulence* (Cambridge University Press, Cambridge, England, 1995).
[2] S. Lovejoy, Science **216**, 185 (1982).
[3] R. D. Cess *et al.,* Science **245**, 513 (1989).
[4] A. Davis *et al.,* J. Atmos. Sci. **53**, 1538 (1996); A. Marshak *et al.,* J. Atmos. Sci. **54**, 1423 (1997).
[5] R. F. Cahalan and J. B. Snider, Remote Sens. Environ. Sci. **28**, 95 (1989); S. Lovejoy *et al.,* Ann. Geophys. **11**, 119 (1993); A. Davis *et al.,* J. Atmos. Sci. **54**, 241 (1997).
[6] G. Parisi and U. Frisch, in *Turbulence and Predictability in Geophysical Fluid Dynamics and Climate Dynamics,* edited by M. Ghil *et al.* (North-Holland, Amsterdam, 1985), p. 84.
[7] J. F. Muzy, E. Bacry, and A. Arneodo, Int. J. Bifurcation Chaos Appl. Sci. Eng. **4**, 245 (1994); A. Arneodo, E. Bacry, and J. F. Muzy, Physica (Amsterdam) **213A**, 232 (1995).
[8] (a) J. Arrault *et al.,* Phys. Rev. Lett. **79**, 75 (1997). (b) A. Arneodo, N. Decoster, and S. G. Roux, Eur. Phys. J. B (to be published).
[9] D. Schertzer and S. Lovejoy, J. Geophys. Res. **92**, 9693 (1987); in *Fractals: Their Physical Origin and Properties,* edited by L. Pietronero (Plenum, New York, 1989), p. 49.
[10] A. Marshak *et al.,* Phys. Rev. E **49**, 55 (1994).
[11] B. Castaing, Y. Gagne, and E. J. Hopfinger, Physica (Amsterdam) **46D**, 177 (1990).
[12] A. N. Kolmogorov, J. Fluid Mech. **13**, 82 (1962); A. M. Obukhov, J. Fluid Mech. **13**, 77 (1962).
[13] (a) E. A. Novikov, Phys. Rev. E **50**, 3303 (1994). (b) B. Castaing and B. Dubrulle, J. Phys. II (France) **5**, 895 (1995).
[14] A. Arneodo, J. F. Muzy, and S. G. Roux, J. Phys. II (France) **7**, 363 (1997); A. Arneodo, S. Manneville, and J. F. Muzy, Eur. Phys. J. B **1**, 129 (1998).
[15] S. Mallat and W. L. Hwang, IEEE Trans. Inf. Theory **38**, 617 (1992).
[16] Note that the resolution of our 2D WT microscope does not allow us to investigate the LANDSAT scale break (around 200–400 m) reported in Refs. [5].
[17] G. Ruiz-Chavarria *et al.,* Physica (Amsterdam) **99D**, 369 (1996).